Strong Coupling Expansion for the Nonequilibrium Properties of Ultracold Atoms on an Optical Lattice

J.K. Freericks and K. Mikelsons
Department of Physics, Georgetown University, Washington, DC
{freericks, karlis}@physics.georgetown.edu

H.R. Krishnamurthy
Centre for Condensed Matter Theory, Department of Physics, Indian Institute of Science, Bangalore, India
hrkrish@physics.iisc.ernet.in

Abstract

We describe a new method, based on a strong coupling expansion, to model ultra-cold atoms on an optical lattice in non-equilibrium. The method is ideally-suited for the systems with strong interactions and high initial temperatures, which is often the case for cold atom experiments. We discuss the computational aspects of this method, including precision, accuracy, scaling and numerical implementation. We present results for fermionic atoms in a strong homogeneous electric field, showing the Bloch oscillations of the current and the evolution of the momentum distribution in time.

1. Introduction

The field of ultra-cold atoms has been growing extensively over the past few years. One of the reasons why this is so is that these systems are clean and tunable and, hence, have the possibility for providing direct testing of theoretical predictions. Richard Feynman proposed using controllable quantum mechanical systems for analog quantum computation, allowing the system to evolve, and then reading out the results of the quantum mechanical system (Feynman, 1982). While simple in principle, carrying out such a project is a daunting task full of many technical challenges. Defense Advanced Research Projects Agency (DARPA) is sponsoring a program on creating just such an optical lattice emulator, employing ultra-cold atoms within an egg-carton-like potential created by retro-reflected laser beams, and simulating the presence of a periodic potential of real materials. Nearly all experiments currently carried out work in non-equilibrium, where the system is driven by some kind of external disturbance and then has its properties measured to learn more about the system. The goal of this work is to properly simulate this non-equilibrium aspect by using strong-coupling perturbation theory. While much progress has been made on equilibrium problems, there is limited work on the non-equilibrium dynamics of such strongly correlated systems and, hence, little is known about their behavior. We show in this work that one can solve these problems with an approximate method well-suited to the cold-atom experiments.

2. Numerical Method

Our theoretical approach is based on the so-called strong-coupling expansion (SCE). The SCE has been used for a variety of problems with good success, and can be considered as a fairly established technique, especially in the equilibrium. Early efforts of the strong-coupling expansion for cold-atoms focused on the equilibrium properties of the Bose-Hubbard model (Freericks and Monien, 1996; see also Freericks, et al., 2009). Applications to the Fermi-Hubbard model have showed that they also work very well in the high-temperature regime (Jördens, et al., 2008 and 2010).

The Fermi-Hubbard model (Hubbard, 1963), is a simplified model of fermions moving on a lattice via hopping, and interacting via an on-site repulsion when two fermions of opposite spin occupy the same lattice site (two fermions of the same spin cannot occupy the same lattice site due to Pauli blocking from the Pauli exclusion principle). The Hubbard model can be described by a simple Hamiltonian as follows:

$$H(t) = -J(t) \sum_{<ij>,\sigma} \left(e^{i\vec{A}(t)\left(\vec{r}_i - \vec{r}_j\right)} c^{\dagger}_{i\sigma} c_{\sigma j} + h.c. \right) + U(t) \sum_i n_{i\uparrow} n_{i\downarrow},$$

where

- $J(t)$ is the hopping amplitude between the nearest-neighbor sites on the optical lattice,
- $U(t)$ is the on-site repulsion between two atoms in different hyperfine spin-states on the same optical lattice,
- $\vec{A}(t)$ is the vector potential determined by the electric field: $\vec{A}(t) = \int_0^t \vec{E}(t')\,dt'$,
- $c_{i\sigma}^{\dagger}$ is the creation operator for a particle at site i and in the hyperfine spin-state σ,
- $n_{i\sigma}$ is the number operator given by $n_{i\sigma} = c_{i\sigma}^{\dagger} c_{i\sigma}$,
- $\vec{r}_i$ is the position of the site i.

The first term represents the kinetic energy due to the hopping of the particles, while the second term is the potential energy due to interactions between the particles. In general, the hopping magnitude, the on-site repulsion and the electric field can be time-dependent within this model. It turns out that this model can be created in a straightforward way in experiments on ultra-cold fermionic atoms with two hyperfine states, such as Li^6 or K^{40}.

For systems where the interactions between atoms are strong, they tend to impede the movement, or hopping of the particles, and the atoms are nearly localized. This occurs because there is only one atom occupying a given lattice site at a given moment in time, and if we have on average one atom per site, the motion is frozen out due to the fact that doubly occupying a lattice site is forbidden by the strong repulsive interaction. These are precisely the conditions in many experiments of ultra-cold atoms on optical lattices. The basic idea of the SCE is to start with the local (or atomic) problem (with zero hopping), which can always be easily solved, and proceed to calculate the corrections as increasing orders in expansion in the hopping. Our focus in this work is on fermionic atoms on an optical lattice, which are described by the Fermi-Hubbard model and can be used to model a number of other physical systems.

The basic quantity that is calculated in many-body physics is the Green's function, which measures the quantum-mechanical amplitude and phase for creating a particle on one lattice site at time t_2 and destroying it at a different lattice site at time t_1:

$$G_{ij}(t_1,t_2) = -i\left\langle T_c c_i(t_1) c_j^{\dagger}(t_2)\right\rangle = -i\frac{\mathrm{Tr}\left[T_c e^{-\beta H(t=0)} c_i(t_1) c_j^{\dagger}(t_2)\right]}{\mathrm{Tr}\left[e^{-\beta H(t=0)}\right]}$$

The thermal average in this formula is performed with respect to the original Hamiltonian at time t=0 and T_c denotes contour ordering of the creation and annihilation operators (see below). All operators are expressed in the Heisenberg picture. The non-trivial quantum-mechanical effects in the Green's function are recorded in the so-called self-energy (which determines how the interactions shift the energies of the quantum states, and how long those states live as coherent excitations). In a non-equilibrium theory, the self-energy becomes of critical importance if one wants to study relaxation or damping effects, because one needs to have a theory that can accurately determine it in order to properly determine the damping. The self-energy is defined as:

$$\boldsymbol{\Sigma} = \mathbf{G}_0^{-1} - \mathbf{G}^{-1}$$

This definition of the self-energy in the SCE is similar to the conventional (weak-coupling) definition, except that here $\mathbf{G_0}$ is the atomic (not the non-interacting) Green's function. In the simplest picture, this quantity describes a correction to propagation of the atom due to hopping to a neighboring site on the optical lattice and then returning back.

The calculation of non-equilibrium properties is complicated (as compared to an equilibrium calculation), since the absence of the time translation invariance implies that the Green's functions and self-energy describing the system are now continuous matrix operators in two time-variables, defined on the so-called Kadanoff-Baym-Keldysh contour. This contour starts at an early time, runs to a maximal simulated real-time, then back to the early time, and finally includes an imaginary time-branch that is necessary for the initial thermalized boundary condition of the system before the field is turned on (and whose length is given by the inverse of the initial temperature of the system). The time-ordering is with respect to the ordering along the contour, implying that later times on the contour occur on the lower branch rather than the upper branch, which is an earlier time. The Kadanoff-Baym-Keldysh contour is shown in Figure 1 in a discretized form with N_t time-steps, because we need to discretize the continuous matrix operators into discrete matrices in order to perform numerical calculations. Thus, the matrix dimension grows linearly with the maximal simulated real-time. The equations of motion become matrix equations and their solution requires operations with large matrices (such as inversion, contraction with a higher rank tensor, etc.), drastically increasing the computational complexity of the problem.

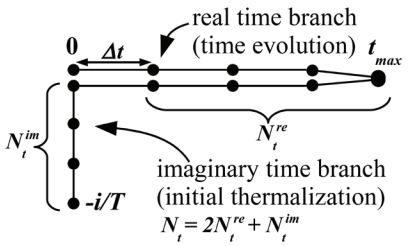

Figure 1. Kadanoff-Baym-Keldysh contour. The non-equilibrium evolution of the system is described by the real-time branches. The imaginary-time branch accounts for the initial thermalized boundary condition of the system. For computational purposes, the contour gets discretized into $N_t = 2N_t^{re} + N_t^{im}$ time-steps.

We now sketch the algorithm used to solve this problem. The atomic problem can always be directly solved to obtain the atomic Green's function. Once that is done, we formulate a series expansion in powers of the hopping (Freericks, et al., 2009). We include terms up to second-order in the hopping, which corresponds to atoms i) hopping once to a neighboring site; ii) atoms hopping twice and ending up two sites away; and iii) atoms hopping to a neighboring site and returning to the original site (see Figure 2). Truncation of terms beyond the second-order is required due to the rapidly growing computational complexity, and results in an often unsatisfactory approximation, as it does not allow for atoms to propagate further than two sites away from the original one. Fortunately, it can be significantly improved by a partial but infinite resummation of terms, which results in a better treatment of the long-range propagation. This level of resummation of terms results in a matrix inversion to solve the linear matrix equation of motion for every point in momentum space (Dyson's equation). The second-order contributions to the propagation can be grouped and expressed through the so-called second-order local cumulant self-energy (further denoted as simply the self-energy). This second-order contribution is especially important in non-equilibrium, as it is required to model relaxation processes, whereby an initially perturbed system relaxes to a stationary long-time solution. Furthermore, we require that in a homogeneous system, the propagation of atoms on the neighboring site is governed by the same Green's function as on the original site. This approximation results in a self-consistency requirement whereby the self-energy depends on the local Green's function, which, in turn, depends on the self-energy. We solve the resultant system of non-linear matrix equations iteratively by choosing a starting approximation (such as taking the local Green's function equal to the atomic Green's function), and proceeding with the self-consistency loop, where sequential iterations produce a more accurate estimate for the unknown quantities. Usually, about ten self-consistency iterations are necessary to reach convergence. The total energy and the potential energy can be obtained from the equal time derivative of the converged local Green's function. Finally, the calculation needs to be repeated for different degrees of time discretization to estimate the systematic error associated with the finite number of time-steps.

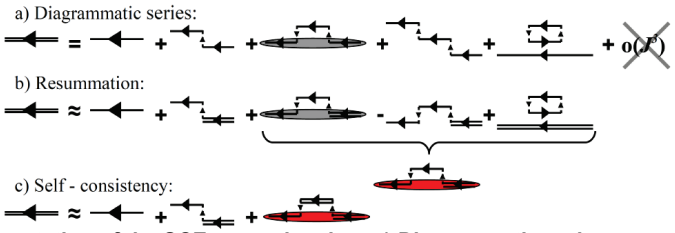

Figure 2. Diagrammatic representation of the SCE approximation: a) Diagrammatic series up to second-order in hopping with higher-order terms truncated. A single line denotes the atomic Green's function, a double line denotes the full Green's function and a dashed line indicates hopping to a neighboring site. The gray shaded oval denotes the two particle local atomic Green's function (Equation 13 in Freericks, et al., 2009). b) Resummation of the diagrams giving rise to Dyson's equation. The second-order term that represents hopping two sites away is generated by the resummation of the first-order term, yet this resummation introduces another local second- order term. The three second-order terms (Equation 23 in Freericks, et al., 2009) can be grouped together into a single-term that involves the two particle cumulant Green's function (red shaded oval; Equation 24 in Freericks, et al., 2009). c) The self-consistency requirement implies that the propagation on the adjacent site in the second-order term is the same as the full Green's function.

The basic algorithm is depicted in Figure 3: i) we start with calculating the atomic Green's function and setting the initial guess for the local Green's function equal to that; ii) we compute the self-energy by evaluating the terms through second-order of the SCE; and iii) we find the momentum dependent Green's function by solving Dyson's equation [this is accomplished by finding the inverse of an $N_t \times N_t$ matrix for each momentum value] and sum them to obtain the local Green's function. Quantities such as the current and average kinetic energy are measured during this step. This loop

[steps (ii)–(iii)] is iterated until the quantities converge. To facilitate the convergence of this iterative process towards a stable physical solution, we introduce a linear mixing parameter for the self-energy, which controls the fraction of the updated self-energy used in the following iteration. Decreasing this parameter stabilizes the self-consistency cycle at the expense of slower convergence. We find that value of 0.5 for this parameter to be adequate for most of our calculations. This results in an exponential convergence towards the stable solution with approximately 10–20 iterations needed to decrease the relative change in self-energy between two successive iterations to less than 10^{-3}.

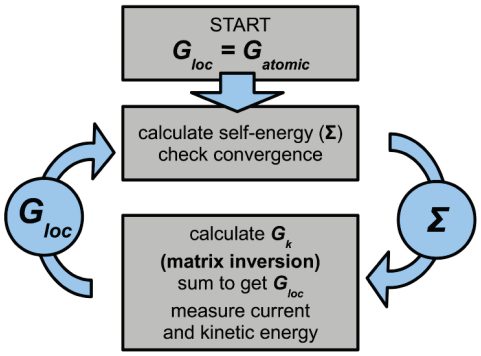

Figure 3. Schematic of the self-consistent, strong-coupling expansion algorithm for homogeneous problems. The calculation of the local Green's function from the local self-energy is a large matrix problem that does not simplify via Fourier transformation. Calculation of the local self-energy is a more expensive operation, but it is easy to parallelize.

The SCE in non-equilibrium has the same limitations as its equilibrium counterpart: it only works if the interaction to hopping ratio is sufficiently large and if the initial temperature is not too low. When these conditions are violated, we see a decrease in the accuracy of the SCE results that is accompanied by a slower (or ultimately failing) convergence of the self-consistency cycle. Normally, the SCE converges down to temperatures smaller than the hopping. This implies that the SCE works very well within the parameter regime of current experiments with ultra-cold atoms on optical lattices.

3. Scaling of the Numerical Algorithm

The algorithm has two natural parallelizable pieces. The first is the solution of the Dyson's equation to solve for the momentum-dependent Green's function. This needs to be done for each value of momentum in the discretized reciprocal (or momentum) space. We use the complex matrix inversion routines ZGETRF and ZGETRI from LAPACK software libraries (Anderson, 1999) for the matrix inversions. Each core performs one matrix inversion at a time, and the contributions to the local Green's function and other measurements are then added together. This part of the algorithm scales as N_t^3 and takes about 5–20% of the total computation time. The number of points in reciprocal space can be adjusted (by choosing an appropriate discretization of reciprocal space) to be a multiple of the number of cores for better scaling.

The other parallel part is finding the self-energy. This is the most expensive part of the algorithm, as it scales as N_t^4. Calculating each element of the self-energy matrix requires $o(N_t^2)$ operations and is computed on a single processor. Usually, we choose both N_t and the number of processors to be powers of two, so that the total number of matrix entries (N_t^2) is always a multiple of the number of processors (also a power of two). We use the BLAS software library (Blackford, 2002) for this part of algorithm. Because the contribution to the self-energy matrix involves calculation of the two-particle Green's function, which is a rank-four tensor and depends on four time-indices and their relative sequential order (and thus there are 24 possible time-orderings), it is not possible to formulate the calculation of the self-energy as a BLAS Level 3 call (matrix–matrix operation). Instead, calculation of a single element of the self-energy matrix uses the BLAS Level 2 routine ZDOTU for a dot product of a range of values of the Green's function, and appropriate lookup arrays for the calculation of the two-particle Green's function.

Aside from these two computationally-expensive steps of the algorithm, the remaining operations add little overhead. Initialization of the data, as well as output of the results usually takes less than 1% of the execution time. Due to the extremely-parallel nature of the calculation, the code runs quite efficiently on parallel machines, with only up to around 1% of the total time spent for communications (see Figure 4).

We illustrate the efficiency of the code by examining the scaling with the number of processors and scaling with the problem size. We start with the strong scaling results in Figure 4. We run the same code on different numbers of processors, chosen to be a fraction of the maximal number of processors needed for a given run. The code shows good linear scaling for small numbers of processors, and fitting the lowest four data points to a line produces the theoretical maximal scaling (red dashed) line shown in the figure. The performance of the actual code lies at about 94% of linear scaling on 4,096 processors, which is excellent performance. The code does not have a significant serial part in the main loop, which is why it scales so well.

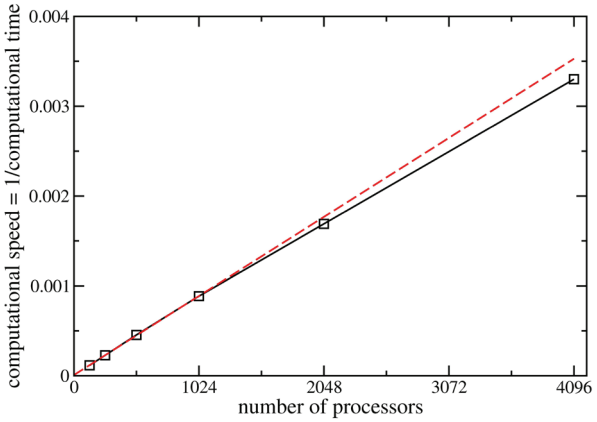

Figure 4. Strong-scaling plot for the SCE algorithm. We achieve 94% of linear-scaling on 4,096 processors. This is an excellent strong-scaling result. These results were obtained for a sample calculation for one iteration of the self-consistency loop with N_t=2,048 time-slices and N_k=32,768 points in momentum space on the AFRL Cray XE6 (raptor).

In Figure 5, we show the results for scaling with the problem size. The code is run for different numbers of time-slices corresponding to simulating different intervals of physical time, as well as different levels of time discretization for a fixed-time interval. Results with different levels of time discretization can be used to assess the error due to the discretization. As expected, most of the computational time is spent calculating the self-energy, which shows a consistent N_t^4 scaling with the number of time-slices. The other computationally-extensive part of algorithm, calculation of the local Green's function, scales as N_t^3 for a fixed-number of momentum points. This part of code scales strictly linearly with increasing the number of momentum points.

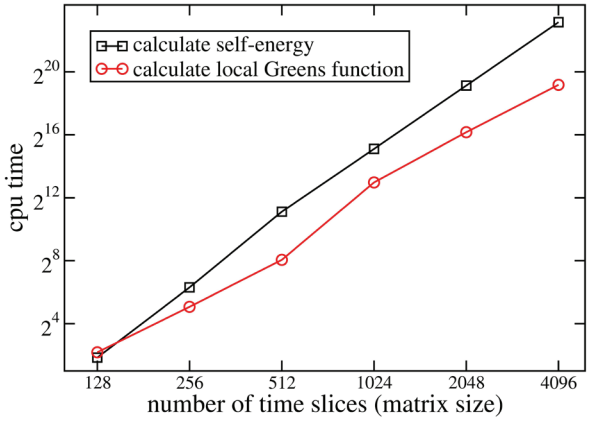

Figure 5. Scaling comparison for two main operations of the self-consistent SCE algorithm on the Cray XE6 (chugach) (at DoD HPCMP Open Research Systems). The dominant part of the calculation is taken to calculate the self-energy, which scales as N_t^4. Calculation of the local Green's function involves inversion of matrices, and thus scales as N_t^3 (A kink in this scaling is due to a better cache utilization for smaller matrices). Using this scaling, we can reliably predict the computation time for even longer times (more time-slices). The number of points in momentum space is N_k=4,096. The number of processors range from 4 (N_t=128) to 2,048 (N_t=4,096), so these results represent good weak-scaling behavior. (Note these results are not plotted in the conventional weak-scaling method, since we show the number of time slices, not the number of processors on the horizontal axis, and the plot is a log-log plot.)

The algorithm is highly-efficient for two reasons: i) the communications is kept to a minimum, as we only have two Message Passing Interface (MPI) matrix reduction and distribution calls per self-consistency iteration, and ii) the matrix operations are handled with LAPACK and BLAS codes that are highly optimized for each processor.

4. Results and Discussion

As an example application, we study fermionic cold-atoms on a three-dimensional optical lattice with the simulated electric field aligned along the diagonal direction (1,1,1) of the lattice (we examine a periodic system, so we do not include the trap potential for the atoms, which makes the system inhomogeneous). In general, our method is not restricted to any number of dimensions or lattice geometries, but we expect it to work better in higher-dimensions, and the three-dimensional problem is the largest computational problem in terms of lattice size and number of particles, so we focus on that case. We study a homogeneous system with number of atoms equal to the number of optical lattice sites ("half-filling"). The "electric field" within the context of the cold-atom experiments can be created in two different ways: i) a linear potential can be added, whose slope is the magnitude of the electric field, or ii) the lattice potential can have the two retro-reflected beams shifted in frequency, so the system has a standing wave in a moving frame, and the lattice is pulled through the cloud of atoms (with the rate of pulling being proportional to the electric field). In equilibrium, a strongly interacting system at half-filling is characterized by a "Mott-insulating" state (Mott, 1949), where the hopping of particles is strongly suppressed due to the energy penalty for two particles to occupy the same lattice site. In this study, we keep the interaction U and the hopping J fixed, so that the time-dependence of the problem comes due to the electric field being switched on.

As a first result, we show the effect of a time-independent field to produce Bloch oscillations in the current and the corresponding density distributions. Bloch oscillations arise as a response of a periodic system to a time-independent field, due to the electric field shifting the momentum of atoms at a constant rate and momentum being reflected off the Brillouin zone boundaries when the momentum reaches the edge of the Brillouin zone (Bloch, 1929). The frequency of the Bloch oscillations is determined by the strength of the electric field, while the amplitude is determined by the initial density distribution (itself a function of temperature) and various other factors (such as the interactions) that determine the relaxation of the system to a stationary state.

In Figure 6, we show the resultant Bloch oscillations in the current after an application of a relatively strong time-independent field E=4.0 (in the units of the on-site repulsive interaction U between the atoms) for three values of the initial temperature. The current shows rapid oscillations, with period $2\pi/E$. As expected, the amplitude is higher for the lower-temperature cases. The amplitude modulation has a period determined by the interaction U.

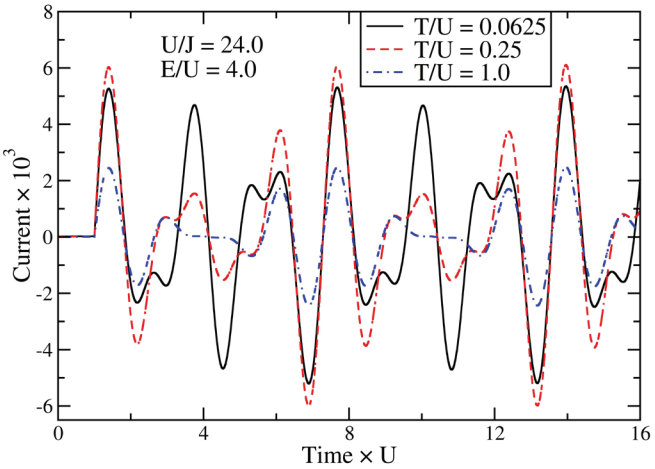

Figure 6. Plot of the current after a constant time-independent electric field E=4.0 is switched on at time *t*=1.0. The current shows Bloch oscillations with the frequency determined by the strength of the field and increasing amplitude with lower- temperature. The oscillations do not show a significant damping, but do have an overall amplitude modulation. The system is a 3D optical lattice half-filled with fermion cold-atoms, so that on average there is one atom per site. The electric field is aligned along the diagonal (1,1,1) direction of the lattice.

The Bloch oscillations also manifest themselves in the expectation value of the total energy. However, since the total energy is obtained from the equal time-derivative of the Green's function, it has a comparatively large dependence on the time-step used in the simulation. More precise data can be obtained by repeating the calculation for at least two different

values of the time-step, and by performing a scaling of the data towards the limit of zero time-step (see Figure 7). For strong-fields, the change in the total energy at short-times is almost entirely due to the changing kinetic energy, whereas the potential energy (due to doubly occupied sites) increases much more slowly.

The change of the total energy is due to Joule heating caused by the finite current after the field is turned on. This dissipated energy can be calculated by integrating the current times the field. Since we have obtained the data for the total energy and the current independently, we can verify how well our results satisfy total energy conservation (see Figure 8). Here, we show data for the case when field is equal to the interaction. In this case, the total energy grows rapidly and oscillates around the infinite temperature equilibrium value of $U/4$. The current shows a single peak responsible for the heating of the system. The total energy obtained by integrating the current times the field agrees well with the data obtained from the derivative of the Green's function, yet there is a constant offset at long-times. The agreement between the measured current and the current obtained from the time-derivative of the total energy is better, but not perfect. Since extrapolated data are used in Figure 8, it is likely that the slight disagreement in energy conservation is due to the nature of the approximation, which does not include all of the terms in the strong-coupling expansion, or it might be that the step-size was not small enough to be in the scaling regime and allow us to accurately go to the zero step-size limit. The energy conservation for larger values for field is considerably better than the $E=U$ case.

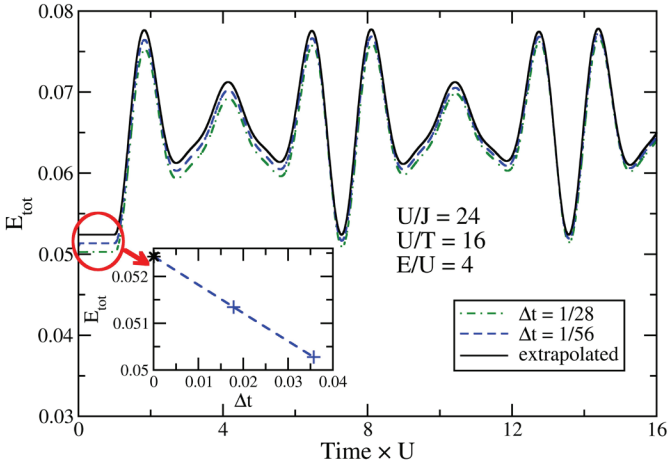

Figure 7. The total energy for hopping *U/J*=24, temperature *U/T*=16 and field *E/U*=4. Data for two different values of time-steps are used to extrapolate towards the $\Delta t \rightarrow 0$ limit. The inset shows scaling with the time-step size of the total energy at an early time before the field is turned on. The extrapolated data in this case coincide with the equilibrium value of the total energy obtained by simulating a very-short time-period with zero-field (black star in the inset).

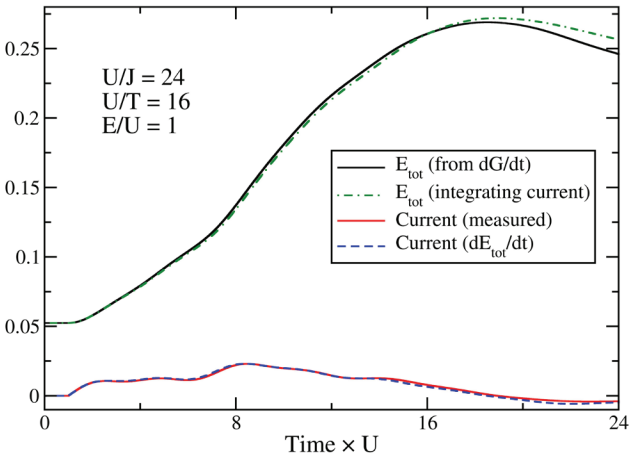

Figure 8. Energy conservation: The energies obtained from the derivative of the Green's function (solid black line) and by integrating the current time-field (green dash-dotted line) show a very good agreement; however, at long-times there appears to be a constant energy shift. Alternatively, one can compare the measured current (solid red line) with the one obtained by differentiating the total energy with time (dashed blue line) – these data show a better agreement, with small differences at some regions where the current changes most rapidly.

Another way to test to accuracy of the calculation is to compare the data for the spectral moments to the exact theoretical values. The spectral moments are linked to the derivatives of the retarded Green's function, and this relation also holds in the non-equilibrium. Furthermore, the exact values for these moments can be found (Turkowski and Freericks, 2006). The zeroth spectral moment is simply the integral of the spectral function, which is equal to one. The first moment is zero for a half-filled system due to the particle-hole symmetry, which means that the spectrum is an even function. The expression for the second moment is $U^2/4+6J^2$ for a three-dimensional (3D) system at half-filling. In Figure 9, we compare our results for the zeroth and second spectral moments (obtained from the retarded Green's function) with the exact values. In both cases, the small deviations from the exact values vanish as the results are scaled towards the limit of zero time-step size. The scaling towards the exact values is quadratic in the time-step size.

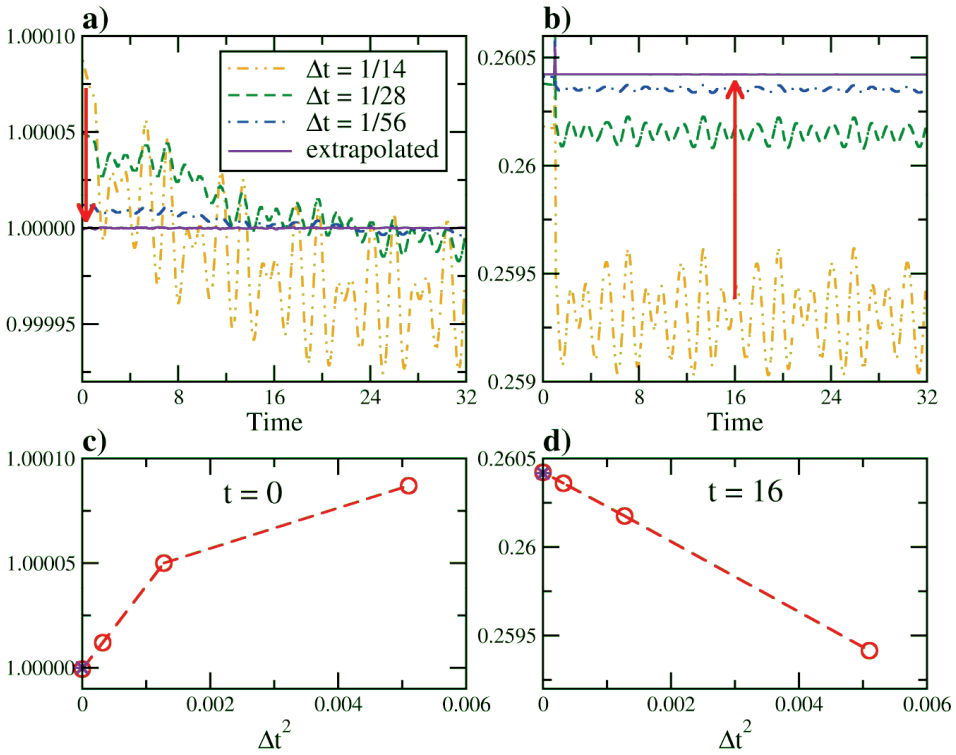

Figure 9. Scaling of the spectral moments for *U/J*=24, *U/T*=16 and *E/U*=4. a) and b): zeroth and second spectral moments for three values of the time-step. For a finite-time-step, the moments slightly deviate from the exact value and slightly vary with time. The extrapolated values match perfectly with the exact value for the whole time interval. c) and d): scaling of the zeroth and second moments towards the $\Delta t \rightarrow 0$ limit. Both cases show a perfect scaling with Δt^2 for small Δt and a perfect agreement between the extrapolated and the exact values.

Finally, we show the gauge-invariant momentum distribution of the atoms in Figure 10 (Bertoncini and Jauho, 1991). In the case when the field is along the diagonal of the lattice, the momentum distribution of a 3D system (normally dependent on three momentum projections) can be parametrized by only two variables: $\varepsilon=-2[\cos(k_x)+\cos(k_y)+\cos(k_z)]$ (related to band-energy) and $\eta=-2[\sin(k_x)+\sin(k_y)+\sin(k_z)]$ (related to the component of the velocity along the direction of the field), and in the (ε,η) plane all momentum points fall within a circle with radius 6. Initially, before the field is switched on (at time t=1.0), the system is in equilibrium, and the momentum distribution only depends on the "band-energy" variable ε. After the field is switched on, the distribution starts to rotate with a frequency determined by the Bloch oscillations. With time, the range of variation in the momentum distribution changes following the modulation of the Bloch oscillations in the current.

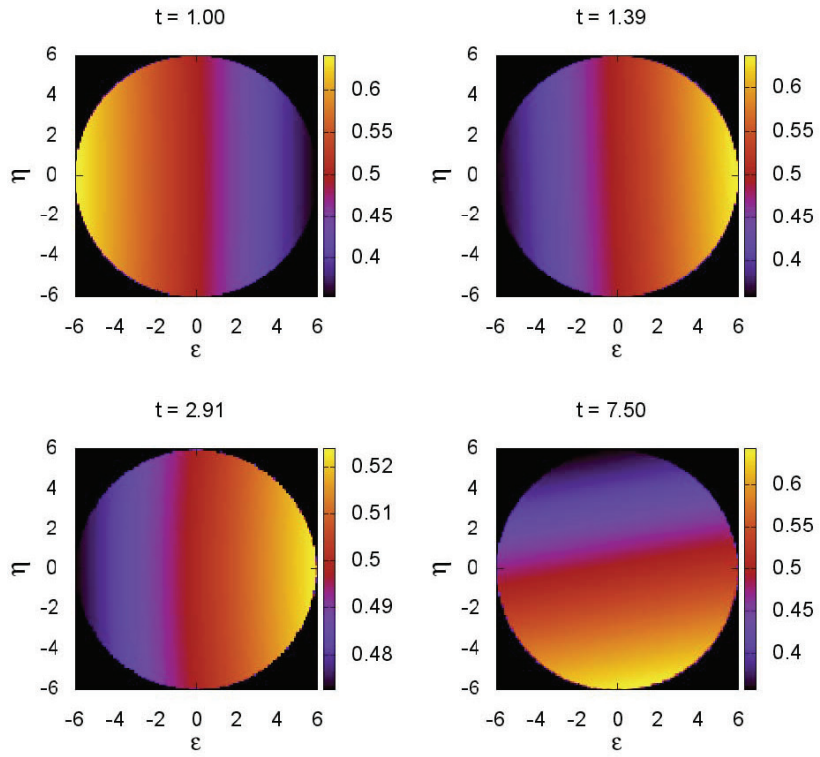

Figure 10. Momentum distribution of the atoms after a time-independent electric field (E=8.0) is switched on at time *t*=1.0. The momentum distribution is parametrized by two variables ε ("band-energy") and η ("velocity along the direction of the field"). The top left picture shows the distribution in equilibrium, just before the field is switched on. The rest of the pictures show the distribution at later times, when it is significantly perturbed away from the thermal equilibrium. These changes occur primarily in the rotation of the line dividing high- and low-occupancy and in the fact that range of the occupation changes in time, as can be seen by the changing scales in the panels at long-times.

5. Significance to the DoD

The DARPA-sponsored program for creating an optical lattice emulator has had significant success with equilibrium simulators, showing how such analog quantum computers can work in a wide-variety of different platforms. The next steps beyond this work can go in a number of different directions. One can try to add more realistic materials properties to the models, and use the simulators as a virtual materials design laboratory for discovering smart materials with specified properties; or one can take these systems into the nonequilibrium domain and use them to understand the behavior of these systems under the presence of large driving fields, which is likely to occur in military applications. It is in this latter direction that the current work is moving, and we hope that our techniques will allow us to have more to say in the future on this interesting novel frontier in physics.

6. Conclusion

We have introduced a new method for studying non-equilibrium quantum lattice systems in the strong-coupling regime. This method incorporates the effects of damping that are essential to describe the non-equilibrium behavior. However, this improved approximation has a computational complexity that scales as the fourth-power of the number of points in simulated-time interval and, hence, must be limited, in the end, to rather short times. We survey the essential parts of the algorithm and show how an efficient parallel implementation can be achieved. We have investigated the Bloch oscillations in the case of a strong field and large interactions. We also showed the evolution of the momentum distribution due to the presence of a driving field. Since the time-dependence of parameters can be arbitrarily varied, this method can readily be used to simulate a number of different experiments with cold-atoms. Future work will involve extending this method to treat inhomogeneous systems to include the trap, and also to model bosonic particles.

Acknowledgments

JKF acknowledges support from the Army Research Office Grant Number W911NF0710576, with funds from the DARPA OLE program. JKF and KM were also supported by the AFOSR under the MURI program from grant number FA9559-09-1-0617. JKF also acknowledges the McDevitt bequest at Georgetown. HRK acknowledges support from the DST (India). The collaboration between the US and India was supported by grant number JC-18-2009 of the Indo-US Science and Technology Forum. DoD HPC computer time was provided on Cray XE6 machines located at the US Air Force Engineering and Research and Development Center (AFRL) and the US Army Engineering Research and Development Center (ERDC). More specifically, we used the following machines: chugach, garnet, and raptor. The computational work was supported primarily by the Challenge Project DARPA-C4J.

References

Anderson, E., Z. Bai, C. Bischof, S.Blackford, J. Demmel, J. Dongarra, J. Du Croz, A. Greenbaum, S. Hammarling, A. McKenney, and D. Sorensen, LAPACK Users' Guide, 3rd Ed., *Society for Industrial and Applied Mathematics,* Philadelphia, PA, 1999; see also http://www.netlib.org/lapack/.

Bertoncini, R. and A.P. Jauho, "Gauge-invariant formulation of the intracollisional field effect including collisional broadening." *Physical Review B*, 44, pp. 3655–3664, 1991.

Blackford, L.S., J. Demmel, J. Dongarra, I. Duff, S. Hammarling, G. Henry, M. Heroux, L. Kaufman, A. Lumsdaine, A. Petitet, R. Pozo, K. Remington, and R.C. Whaley, "An Updated Set of Basic Linear Algebra Subprograms (BLAS)." *ACM Transactions on Mathematical Software*, 28-2, pp. 135–151, 2002; see also http://www.netlib.org/blas/.

Bloch, F., "Über die Quantenmechanik der Elektronen in Kristallgittern." *Zeitschrift für Physik*, 52, pp. 555–600, 1929.

Feynman, R.P., "Simulating physics with computers." *International Journal of Theoretical Physics*, 21, pp. 467–488, 1982.

Freericks, J.K. and H. Monien, "Strong-coupling expansions for the pure and disordered Bose Hubbard model." *Physical Review B*, 53, pp. 2691–2700, 1996.

Freericks, J. K., H.R. Krishnamurthy, Y. Kato, N. Kawashima, and N. Trivedi, "Strong-coupling expansion for the momentum distribution of the Bose-Hubbard model with benchmarking against the exact results." *Physical Review A*, 79, pp. 053631-1–22, 2009.

Hubbard, J., "Electron correlations in narrow energy bands." *Proceedings of the Royal Society of London, Series A, Mathematical and Physical Sciences*, 276, pp. 238–257, 1963.

Jördens, R., N. Strohmaier, K. Günter, H. Moritz, and T. Esslinger, "A Mott insulator of fermionic atoms in an optical lattice." *Nature*, 455, pp. 204–207, 2008.

Jördens, R., L. Taruell, D. Greif, T. Uehlinger, N. Strohmaier, H. Moritz, T. Esslinger, L. De Leo, C. Kollath, A. Georges, V. Scarola, L. Pollet, E. Burovski, E. Kozik, and M. Troyer, "Quantitative determination of temperature in the approach to magnetic order of ultra-cold fermions in an optical lattice." *Physical Review Letters*, 104, pp. 180401-1–4, 2010.

Mott, N F., "The Basis of the Electron Theory of Metals, with Special Reference to the Transition Metals." *Proceedings of the Physical Society, Section A*, 62, pp. 416–422, 1949.

Turkowski, V.M. and J.K. Freericks, "Spectral moment sum rules for strongly correlated electrons in time-dependent electric fields." *Physical Review B*, 73, pp. 075108-1–15, 2006; Erratum, *Physical Review B*, 73, pp. 209902(E)-1, 2006.